ANALYSIS OF THE CAVITATING FLOW AROUND THE HORN-TYPE RUDDER IN THE RACE OF A PROPELLER

Jae-Moon Han, Do-Sung Kong, In-Haeng Song
Shipbuilding & Plant Research Institute
Samsung Heavy Industries Co., Ltd., Taejon, 305-380, KOREA

Chang-Sup Lee
Department of Naval Architecture & Ocean Engineering
Chungnam National University, Taejon, 305-764, KOREA

Abstract

This paper describes numerical methods by a mixed formulation of the boundary value problem (BVP) for the prediction of the cavitating flow around the horn-type rudder working behind a propeller. The blade BVP is treated by the classical vortex lattice method, whereas the rudder BVP is solved by the surface panel method. The three-dimensional flow around the rudder and the propeller is computed simultaneously, considering the interactions between them. A modified kinematic boundary condition is applied to predict the mean velocity and flow volume through gap flow region of the horn-type rudder. To validate the numerical scheme, an experiment is performed in large cavitation tunnel. The surface pressure distributions and cavity patterns on the horn-type rudder are investigated and compared with computational results, showing good agreement with measured results.

1 Introduction

As the need of container ships of high capacity grows, the hydrodynamic loading upon propellers and rudders is continuously increasing. This often induces the serious problem of cavitation erosion on propeller blades and rudder surface. The accurate analysis of the flow around a rudder operating behind the propeller is very difficult. The assessment of cavitation performance of a rudder, therefore, generally relies on empirical formulas(Brix 1993). The reliability of such a simple method is often questionable.

The hydrodynamic interaction between propeller and rudder is of great importance because of its effect on practical problems. Many attempts have been made to analyze the propeller-rudder interaction problem. Molland(1981) performed a wind tunnel experiment on rudders operating behind a propeller without a ship hull. A systematic series test for various propeller-rudder configurations was carried out with a zero rudder angle by Stierman(1989). Tamashima et al(1993) used the simplified propeller theory to calculate the performance of propellers, and the panel method was adopted to calculate the forces acting on the rudder. In Han et al(1999), authors also developed a numerical method to analyze the propeller-rudder interaction, and the calculated results were compared to those of experiments.

This paper describes numerical methods for prediction of the cavitating flow around the horn-type rudder working behind a propeller. The numerical method uses a surface panel method to solve the flow around the rudder and a vortex lattice method to solve the flow around the propeller, respectively. The three-dimensional flow around the rudder and the propeller is computed simultaneously, considering the interactions between them. A modified kinematic boundary condition is applied to predict the mean velocity and flow volume through gap flow region of the horn-type rudder. The surface pressure distributions and cavity patterns on the horn-type rudder are calculated and compared with those of experimental results at Samsung Ship Model Basin (SSMB).

2 Numerical Methods

Let us consider a horn-type rudder working behind a propeller with constant rotational speed n as shown in Figure 1. The fluid is assumed to be inviscid, incompressible and irrotational. A Cartesian coordinate system is chosen, i.e. the x-axis coincides with the shaft centerline, defined positive downstream, the positive y-axis points upward, and z-axis completes a right-handed coordinate system. The rudder angle δ_R is defined positive when the rudder is rotated with the leading edge of rudder toward the port side of the ship.

Conservation of mass to the fluid volume leads to the governing equation for the perturbation potential ϕ as follows:

$$\nabla^2\phi = 0 \tag{1}$$

Applying the Green's theorem with the Laplace equation (1), the perturbation potential can be expressed as follows:

$$\phi = \int_S \left[-\phi\frac{\partial G}{\partial n} + \frac{\partial \phi}{\partial n}G\right] dS + \int_{S_W} -\Delta\phi_w \frac{\partial G}{\partial n} dS \tag{2}$$

where G is the Green's function. The body surface S is composed of a propeller blade surface S_B, rudder surface S_R and the wake surface S_W is composed of the propeller wake surface S_{BW} and the rudder wake surface S_{RW}.

2.1 Propeller-rudder interaction in non-cavitating condition

2.1.1 Propeller BVP

The propeller BVP is treated by the vortex lattice method of Kerwin & Lee(1978). Circulation and thickness distributions can be discretized using a lattice of chordwise and spanwise line vortex and source elements, respectively. The strengths of the vortices are determined by satisfying the kinematic boundary condition on the camber surface.

In this method, a discretized form of the kinematic boundary condition is employed as follows:

$$\sum_{\Gamma} \Gamma\vec{v}_\Gamma \cdot \hat{n} = -\vec{U}_{in} \cdot \hat{n} - \sum_{Q} Q\vec{v}_Q \cdot \hat{n} \tag{3}$$

where Γ is the constant strength of each bound vortex, Q represents the line sources to model the blade thickness, $\vec{v}_\Gamma$ is the velocity vector induced by each unit strength vortex loop, $\vec{v}_Q$ is the velocity vector induced by each unit strength line source, and $\hat{n}$ is the surface unit normal vector at the control points for the kinematic boundary conditions. The inflow velocity $\vec{U}_{in}$ is the superposition of the effective wake, the rotational velocity with respect to the propeller fixed coordinate system and the rudder-induced velocities.

Due to the action of the propeller, the axial velocity within the propeller slipstream tube is increased and the radius of the tube is contracted. The exact location of the trailing vortex sheet should in principle be determined by satisfying the kinematic and dynamic boundary conditions on the wake surface as a part of the solution. Instead of solving the exact trailing vortex geometry, we will however adopt the model suggested by Greeley & Kerwin(1982).

2.1.2 Rudder BVP

For the calculation of the performance of a rudder, a surface panel method is used. The fundamentals of the surface panel method are described by Lee(1987) and only brief description is given here. The rudder and its wake surface are discretized with hyperboloidal panels, and normal dipoles and sources having constant strength are distributed on the panels. The Kutta condition is applied to eliminate the pressure jump at the trailing edge of the rudder through an iterative process.

For a horn-type rudder, the viscous effect is dominant at the gap between a fixed and a movable part. The objective of this work is not to obtain an accurate local solution in the gap region but to capture the effect of this flow on the global solution. Hence the effect of the gap is represented by the presence of flux.

Consider the flow inside the gap between the forward and the after portion of the horn rudder as shown in Figure 2. The flow in the gap of the horn-type rudder is modeled as Couette flow and the average velocity $(u_\theta)_m$ in the gap can be written as follows(Pyo & Suh 2000):

$$\frac{(\vec{u}_\theta)_m}{|\vec{U}_{in}|} = \frac{12}{Re}\left(\frac{R_0}{h}\right)\left[-\Delta\theta + \sqrt{(\Delta\theta)^2 + \left\{\frac{Re}{12}\left(\frac{h}{R_0}\right)\left(\frac{|\vec{V}_2|}{|\vec{U}_{in}|}\right)\right\}^2}\right] \tag{4}$$

where $\Delta\theta$ is the angular extent in radian between points 1 and 2, h the width of the gap, R_0 the distance from the trailing edge to the middle of gap ($R_0 = (R_1 + R_2)/2$), and Re is Reynolds number ($Re = U_{in}c/\nu$).

The new boundary condition for the gap panels can be satisfied by specifying the source distribution on these panels using the following expression:

$$\frac{\partial\phi}{\partial n} = \vec{U}_{in}\cdot\hat{n} \pm (u_\theta)_m \tag{5}$$

The problem is first solved assuming the gap is completely sealed. The pressure distribution is computed by differentiating velocity potentials. The problem is then solved again with the boundary condition on the gap panels specified by equation (5). The pressures on the rudder are re-calculated and used to update the boundary condition on the gap panels. A converged solution can be obtained within several iteration procedures.

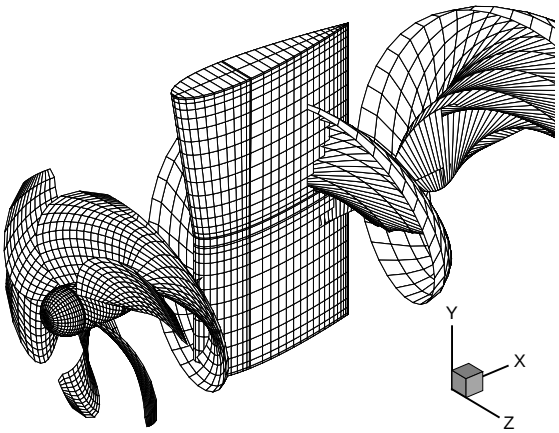

Figure 1: Panel arrangement for propeller-rudder interaction

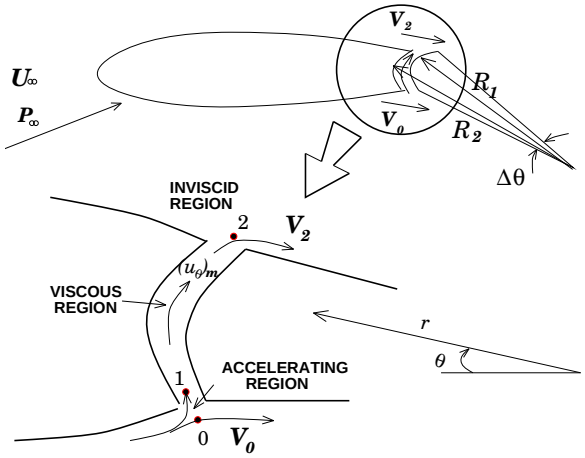

Figure 2: Gap flow model from Pyo & Suh (2000)

2.1.3 Solution procedures

Since we are interested only in the mean performance of the propeller and rudder, the mutual interaction between propeller and rudder may be assumed to be independent of time. The induced velocities in such case are computed at the field points whose angular positions are selected satisfying the rule of Gaussian quadrature, and can be averaged in the circumferential direction.

In the first iteration process, the BVP of the propeller and the rudder may be solved simultaneously for the unknown vortex strength of the propeller and the unknown dipole strength of the rudder. Since the wake geometry of the propeller may be altered due to the presence of a rudder, the wake geometry is re-aligned, considering the influence of the rudder. For this newly determined wake geometry, the BVP of the propeller and the rudder is solved again. The procedure is repeated until the difference in the wake geometry between two successive iterations reaches a preset tolerance. In most of sample calculations, the iteration number of four to six is found sufficient.

2.2 Calculation method for rudder cavitation

When analyzing the cavitating flow around lifting bodies (hydrofoils and propeller blades for instance), the cavitation is assumed to appear on the suction side of the lifting bodies. In the present work, we assume that the sheet cavitation will be present on the port side of the rudder for a right turning propeller (turning clockwise looking forward). The cavitation on the propeller blades is not considered.

The numerical procedure adopted in the present work is similar to that in Kim & Lee(1996). Nonlinear cavity flow problem is linearized by assuming the smallness of the cavity thickness, while the true shape of the rudder section is treated exactly. The cavity extent and shape are determined by satisfying the kinematic and dynamic boundary conditions on the cavity surface, which is collapsed on the rudder surface. See Kim & Lee(1996) for details.

The cavitation number is defined as follows:

$$\sigma_n = \frac{p_{shaft} - p_v}{\frac{1}{2}\rho n^2 D^2} \tag{6}$$

where p_v denotes the vapor pressure, ρ the density, D the diameter of the propeller.

3 Experimental setup

To investigate the validity of the present method, the surface pressure on the horn-type rudder for a container ship is measured in No. 2 test section of large cavitation tunnel of the SSMB (designated herein as SCAT). The No. 2 test section is $3.0m$ wide, $1.4m$ high and $12m$ long. The contraction ratio is 2.8 to 1 and the maximum power at the impeller shaft of $2{,}600kW$ at 120 rpm gives velocities up to $12.0m/s$ in the test section. The maximum free stream turbulence intensity in the test section is 0.5% and the flow uniformity is within 1% for the axial component. The SCAT is able to accommodate the complete model ship as shown in Figure 3, which is used for the powering performance test at the towing tank.

The rudder model is manufactured of aluminum alloy and has an NACA0020 section with geometric aspect ratio $\Lambda = 1.626$ and the balance ratio of 0.256. To measure surface pressure on the rudder, the rudder is fitted with a total of 46 pressure taps, distributed in 4 rows. The locations of these 4 rows are shown in Figure 4. For measurements, a differential pressure transducer is used, which can measure up to 140 kPa. The surface pressure measurements of the rudder are performed in the non-cavitating condition.

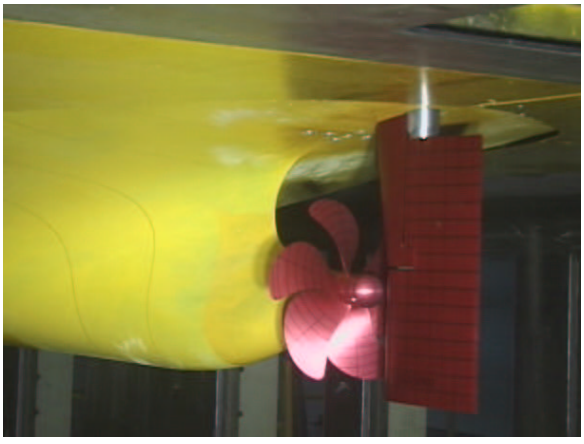

Figure 3: Full model ship mounted in the SCAT

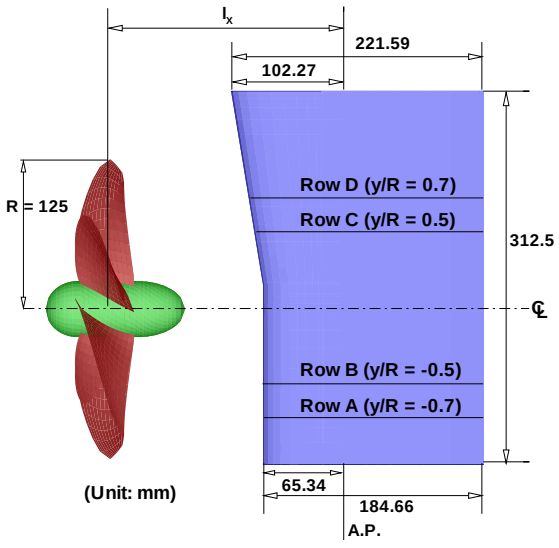

Figure 4: Location of pressure taps

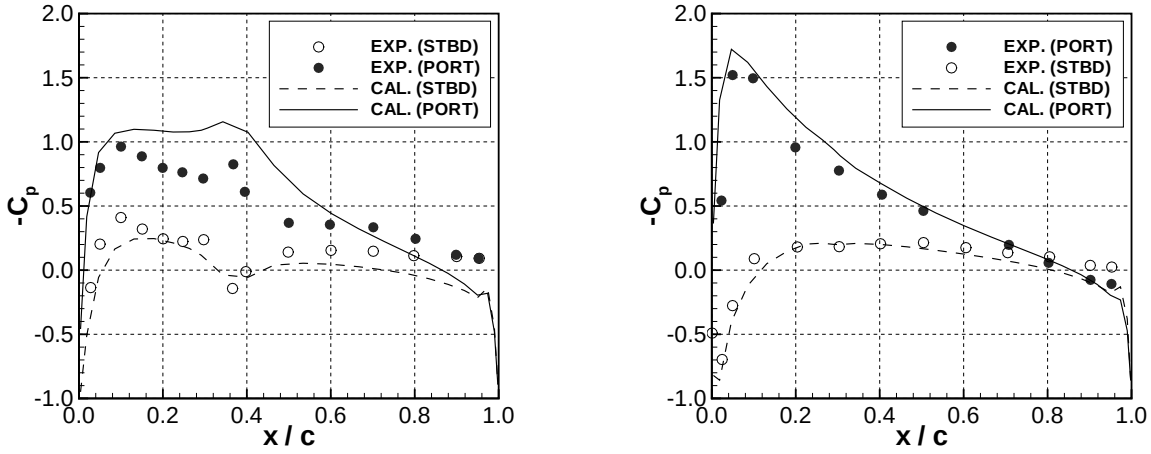

(a) Horn part

(b) Movable part

Figure 5: Comparison of measured and calculated pressure distributions for the horn-type rudder with an NACA0020 section at $\delta_R = 10^o$ in uniform inflow

4 Results and Discussions

4.1 Horn-type rudder in uniform inflow

The method is first applied to the horn-type rudder in uniform inflow. Molland(1981) tested a series of horn-type rudders in a wind tunnel while varying the taper ratio. For the present calculation, No.1 rudder in Molland(1981) is chosen. The rudder has an NACA0020 section with geometric aspect ratio $\Lambda = 1.49$ and the taper ratio of 0.59. Figure 5 shows the pressure distributions predicted by present method together with experimental results by Molland. The rudder is operated at rudder angle $\delta_R = 10^o$. We observe that the correlation with experimental results is reasonably good in the horn part as well as in the movable part.

4.2 Horn-type rudder in the race of the propeller

Sample computations are made with the horn-type rudder in the race of propeller, for which the surface pressure measurement is carried out as described in Section 3. In all cases, the transverse positions of the propeller shaft and the rudder are set on the ship's center plane, i.e. $l_Z/R = 0.0$ and the longitudinal distance from the propeller origin to the pivot point of rudder stock is $l_X/R = 1.5134$. The resulting panel arrangements for the propeller and rudder are shown in Figure 1. All the subsequent computations are performed with $M_P \times N_P = 12 \times 12$ for the propeller and $M_R \times N_R = 32 \times 60$ for the rudder, where M and N denote the numbers of panels in the spanwise and chordwise directions, respectively. For the discretization of the rudder surface, higher panel density is maintained in the vicinity of the gap region.

Figure 6 shows mean velocity distributions in the axial and transverse components together with the corresponding inflow angles along the rudder span. This computation is performed at 5% of the rudder tip chord length upstream from the leading edge of the rudder. The propeller is working at $J_a = 0.714$. The calculated inflow angle entering into the rudder at $y/R = 0.7$ is found to be 7.5 degrees.

Figure 7 shows pressure distributions on the rudder surface at rudder angle 0^o, 8^o and -8^o. Even at $\delta_R = 0^o$, a large suction pressure on the movable part due to inflow angles induced by the propeller appears. In the case of $\delta_R = 8^o$, the extent and the magnitude of the suction pressure is increased. This indicates that cavitation is likely to occur easily on the port side of the rudder for a right turning propeller. The calculated and measured pressure distributions at the horn part ($y/R = 0.7$) and the movable part ($y/R = -0.7$) are compared in Figure 8. In order to compare calculated results with measured ones, the pressure coefficient K_p is defined as follows:

$$C_p = \frac{p - p_{shaft}}{\frac{1}{2}\rho {V_S}^2} \tag{7}$$

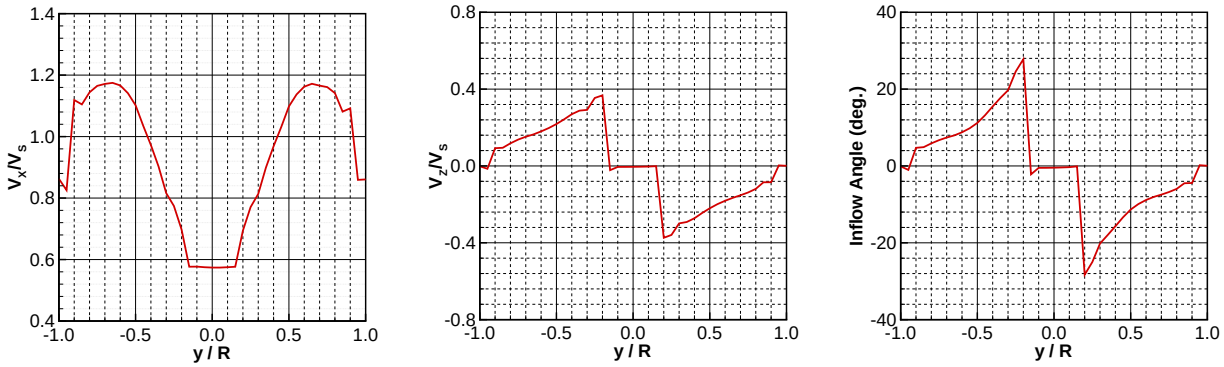

(a) axial velocity (b) transverse velocity (c) inflow angle

Figure 6: Calculated velocities and inflow angles entering into the rudder

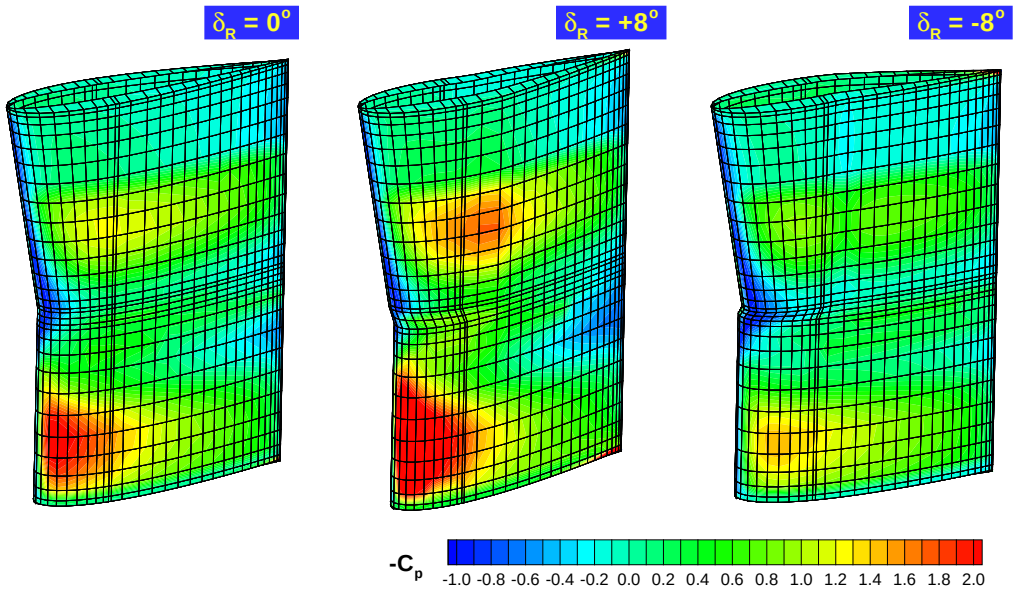

Figure 7: Pressure distributions on the rudder surface with the variation of rudder angle

$$K_p = \frac{p - p_{shaft}}{\rho n^2 D^2} = \frac{1}{2} C_p {J_s}^2 \tag{8}$$

where V_s is ship speed and J_s the advance coefficient based on ship speed ($J_s = V_s/nD$).

At $\delta_R = 0^o$, the pressure distributions on the movable part and the horn part look similar. When the rudder angle is set to 8^o or -8^o, the pressure distributions on the movable part and the horn part differ significantly. At $\delta_R = 8^o$, a large suction pressure peak appears on the port side of the movable part, whereas the suction pressure peak disappears on the horn part because the horn part is not movable. In case of $\delta_R = -8^o$, the pressure distributions on both sides of the movable part is similar. This confirms the calculated result in Figure 6 which predicts the inflow angle of 7.5^o.

4.3 Cavity prediction on the horn-type rudder in the race of the propeller

The numerical method is then applied the cavitating problem of the rudder in the race of a propeller. The panel arrangement is identical to that used in the non-cavitating problem. In Figure 9, the predicted and observed cavity patterns on the horn-type rudder are compared for $\delta_R = 8^o$ with $\sigma_n = 1.613$. The experimental cavity is of bubbly type, whereas the numerical method predicts the sheet cavity. Although the

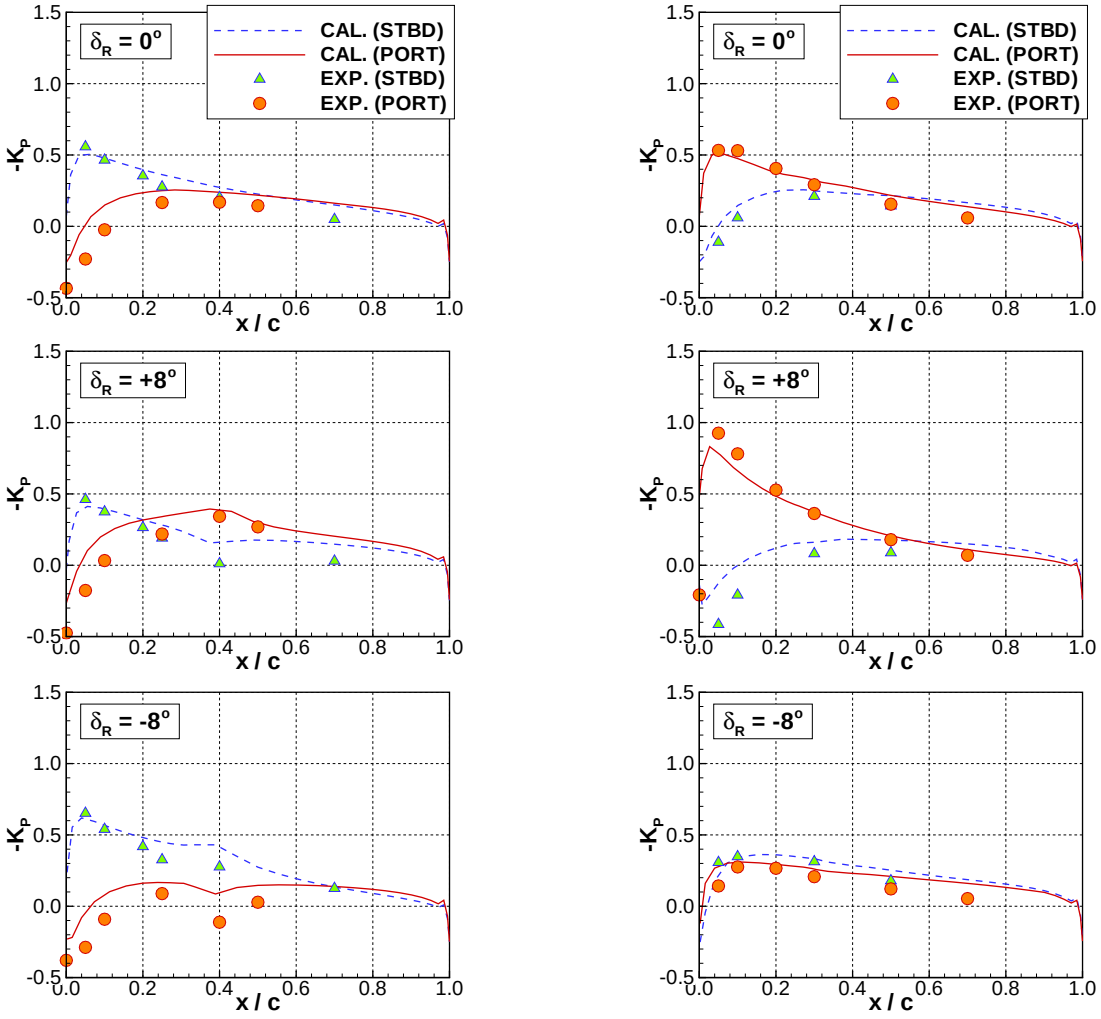

(a) Horn part

(b) Movable part

Figure 8: Comparison of measured and calculated pressure distributions for the horn-type rudder in the race of the propeller with variation of rudder angle

characteristics of the cavity behavior are quite different, the extent of the cavity predicted by the numerical method is very similar to that observed in the experiment. Considering that the present numerical scheme can not handle the bubble-type cavitation, the similarity of the cavity extents indicate that the present numerical method can be used at least to predict the occurrence of the harmful cavity in the design stage.

5 Conclusions

A numerical method for the analysis of the cavitating flow around the horn-type rudder in the race of a propeller is presented. The velocity field upstream of the rudder is calculated and the surface pressure distributions of a horn-type rudder are measured and compared with computational results in the non-cavitating condition, showing good agreement with measured results. Also, the predicted cavity around the horn-type rudder is compared with that of observed result. Although the cavity behavior predicted by the numerical method can not simulate the bubbly-type cavitation, the numerical method is proven applicable to check the likelihood of the harmful cavity (either in sheet-type or in bubbly-type) in the design stage.

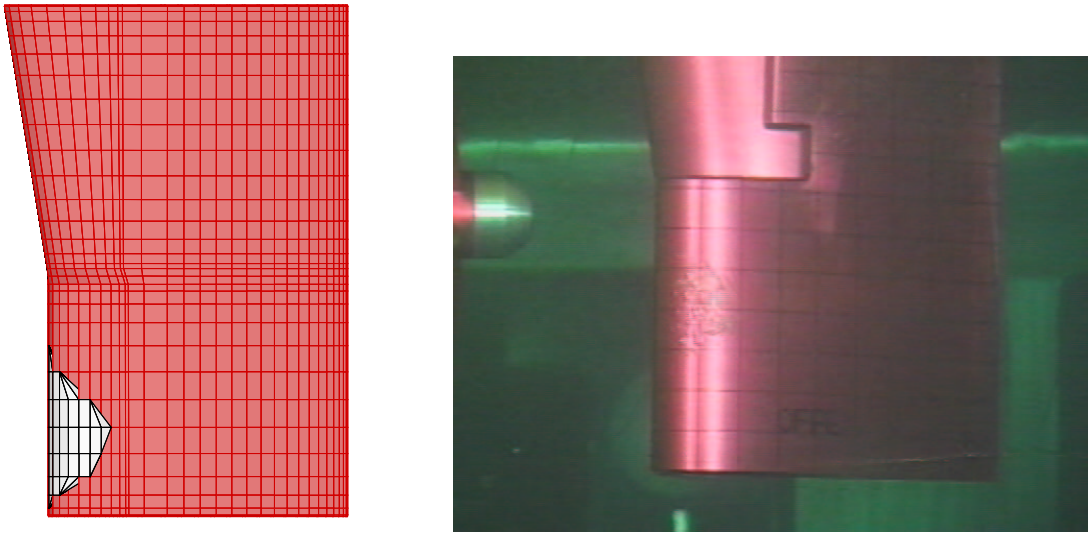

Figure 9: Predicted (left) and observed (right) cavity patterns on the horn-type rudder at $\delta_R = 8^o$ with $\sigma_n = 1.613$

References

Brix, J. 1993 *Manoeuvring Technical Manual.* Seehafen Verlag GmBH, Hamburg.

Greeley D. S. & Kerwin, J. E. 1982 Numerical methods for propeller design and analysis in steady flow. *Trans. SNAME* **90**, 415-453.

Han, J.-M., Kong, D.-S., Kim, Y.-G. & Lew, J.-M. 1999 Analysis of propeller-rudder interaction with rudder angle. *Proceedings*, Annual Autumn Meeting of SNAK, Taejon, Korea, 206-209.

Kerwin, J. E. & Lee, C.-S. 1978 Prediction of steady and unsteady marine propeller performance by numerical lifting-surface theory. *Trans. SNAME* **86**, 218-253.

Kim, Y.-G. & Lee, C.-S. 1996 Prediction of unsteady performance of marine propellers with cavitation using surface panel method. *Proceedings*, 21st Symposium on Naval Hydrodynamics, Trondheim, Norway, 913-928.

Lee, J.-T. 1987 A potential-based panel method for the analysis of marine propellers in steady flow. PhD Thesis, Department of Ocean Engineering, MIT.

Molland, A. F. 1981 The free-stream characteristics of ship skeg-rudders. PhD Thesis, Department of Ship Science, University of Southampton.

Pyo, S.-W. & Suh, J.-C. 2000 Numerical prediction of open water performance of flapped rudders. *Journal of Ship and Ocean Technology* **4**, 1-10.

Shen, Y. T., Remmers, K. D. & Jiang, C. W. 1997 Effects of ship hull and propeller on rudder cavitation. *Journal of Ship Research* **41**, 3, 172-180.

Stierman, E. J. 1989 The influence of the rudder on the propulsive performance - Part I. *International Shipbuilding Progress* **36**, 407, 303-334.

Tamashima, M., Matsui, S., Yang, J., Mori, K. & Yamazaki, R. 1993 The method for predicting the performance of propeller-rudder system with rudder angles and its application to the rudder design. *Transaction of the West-Japan Society of Naval Architects* **86**, 53-76 (in Japanese).